Physical design of a high-charge beam injector for the on-axis swap-out injection scheme in an electron-positron collider

Tongning Hu,[*,†] Hao Hu,[†] Yan Wang, Yifeng Zeng, Di Lu, Kaifeng Liu, and Lanyang Zhang

State Key Laboratory of Advanced Electromagnetic Technology, School of Electrical and Electronic Engineering, Huazhong University of Science and Technology, Wuhan 430074, China

Duan Gu and Xuan Li

Shanghai Advanced Research Institute, Chinese Academy of Sciences, Shanghai 201210, China

Ailin Zhang

Department of Modern Physics, University of Science and Technology of China, Hefei 230026, China

Youjin Yuan

Institute of Modern Physics, Chinese Academy of Sciences, Lanzhou, 730000, China and University of Chinese Academy of Sciences, Beijing, 100049, China

Jingyu Tang[‡]

School of Nuclear Science and Technology, University of Science and Technology of China, Hefei 230027, China and National Synchrotron Radiation Laboratory, University of Science and Technology of China, Hefei 230029, China

(Received 18 November 2024; accepted 21 October 2026; published 6 November 2026)

The Super Tau-Charm Facility (STCF), a next-generation electron-positron collider, adopts an on-axis swap-out injection scheme that demands high-charge electron bunches with exceptionally low emittance and minimal energy spread. This work presents a comprehensive and systematic beam dynamics design for the STCF electron injector. The bunching system, based on subharmonic bunchers and a traveling-wave buncher, is optimized using the nondominated sorting genetic algorithm III to efficiently explore the high-dimensional parameter space. Start-to-end simulations incorporating space-charge forces, wakefield effects, and alignment errors are performed, with beam-based alignment (BBA) applied to correct orbit deviations. The optimized injector delivers 8.5 nC bunches at 3.5 GeV with a normalized transverse emittance below 70 mm mrad and an rms energy spread below 0.5%, satisfying the stringent STCF requirements. The high transport efficiency achieved in simulations alleviates the design pressure on the electron source, while the excellent beam quality inherently suppresses beam halo effects. By integrating systematic multiobjective optimization with high-fidelity simulations, the proposed design overcomes the intrinsic limitations of thermionic cathodes while capitalizing on their proven stability, robustness, and cost-effectiveness, offering an efficient engineering solution for high-charge beam delivery in next-generation colliders.

DOI: 10.1103/89k9-j8qk

I. INTRODUCTION

The particle physics frontiers are to understand the nature of strong interactions, explore matter-antimatter asymmetry, and search for new physics beyond the Standard Model [1,2]. Circular electron-positron colliders at different energy regions represent one of the most effective methods for conducting particle physics experiments and investigating the microscopic world of matter [3–8].

[*]Contact author: tongningHu@hust.edu.cn
[†]These authors contributed equally to this work.
[‡]Contact author: jytang@ustc.edu.cn

Published by the American Physical Society under the terms of the Creative Commons Attribution 4.0 International license. Further distribution of this work must maintain attribution to the author(s) and the published article's title, journal citation, and DOI.

The Super Tau-Charm Facility (STCF) [9], a proposed symmetric electron-positron collider in China, is tailored for tau-charm physics, operating at center-of-mass energies from 2 to 7 GeV. Its ambitious goal is to achieve an unprecedented peak luminosity exceeding 5×10^{34} cm^{-2} s^{-1}. To attain this performance, STCF employs a crab-waist collision scheme, characterized by minuscule vertical beta functions($\beta_y^* \approx 0.8$ mm) and exceptionally low beam emittances (horizontal $\varepsilon_x \approx$ 5 nm rad), colliding up to 2 A of beam current. While these third-generation collider features enable high luminosity, they also introduce formidable nonlinearities and beam-dynamics challenges.

The crab-waist collision mode necessitates the use of crab sextupole magnets to twist the shape of the bunches near the collision point. When combined with the strong focusing around the collision area, it results in an unacceptably small dynamic aperture and momentum aperture of the collision ring. This not only complicates beam injection but also severely shortens the beam lifetime, predominantly restricted by the Touschek lifetime, to less than 300 s [10], significantly shorter compared to other circular electron accelerators. Consequently, the collision ring must operate at a constant current, mandating frequent replenishment of the charge of the circulating bunches. This extremely short beam lifetime poses substantial hurdles for both the beam injection into the collision ring and the design and construction of the injector. Therefore, compared to the off-axis injection scheme that is widely used in currently active light source and collider devices [11–15], STCF has adopted an on-axis swap-out scheme for multi-nC bunches injection, therein, individual bunches within the collider are "in place" replaced by freshly injected bunches [16]. This maintains low emittance and orbit stability but imposes exacting requirements on the injector.

Table I compares STCF's collider-ring injection requirements with those of other storage rings. Evidently, STCF is tasked with injecting multi-nC bunches to achieve extremely high luminosity, a demand far surpassing the capabilities of conventional injectors. Meeting these exacting requirements necessitates an innovative linac-based injector design. The injector must be capable of generating high-charge, ultra-low-emittance bunches at full energy with remarkable stability.

TABLE I. Main performances of the world's colliders [18,20].

Facility	Charge (nC)	Beam energy (GeV)	Luminosity (cm^{-2} s^{-1})
DAΦNE	1.5	0.51	2.4×10^{30}
VEPP-2000	16	1	5×10^{31}
BEPC II	10	2.47	1×10^{31}
SLC (terminated)	11.66	50	6×10^{30}
KEKB	4	8(e^-)3.5(e^+)	4.1×10^{34}
STCF (planning)	8–10	3.5	5×10^{34}

Table I compares the core injection parameters of the STCF collider ring against those of major international colliders: STCF requires injecting 8.5 nC bunches to achieve an ultrahigh luminosity which is comparable to that of KEKB. It should be noted that while STCF adopts a linac-based injection scheme similar to the architectures employed by KEKB and SLC, substantial innovations and improvements are incorporated to address the limitations of these existing facilities.

Note that, unlike the canceled SLC injector, which only achieved 60% of its design bunch charge with low capture efficiency [17], the STCF injector achieves high capture efficiency at 8.5 nC through in-depth optimization. The STCF injector adopts the thermionic-gun architecture with two SHBs and one TW-buncher—a configuration established since SLC [18] and KEKB [19]. While inheriting this proven architecture, the STCF design is distinguished by a systematic optimization methodology: nondominated sorting genetic algorithm III (NSGA-III) efficiently explores the high-dimensional parameter space, and modern computing resources enable increased macroparticle statistics for improved simulation fidelity. The optimized design achieves high transport efficiency without requiring a beam scraper—eliminating the associated charge loss and radiation hazards—while the excellent beam quality inherently suppresses beam halo. These complementary features overcome intrinsic thermionic-cathode limitations while capitalizing on decades of operational experience; combined with advanced optimization algorithms, the full potential of thermionic injectors can be further realized. The collision luminosity of STCF is 4 orders of magnitude higher than that of SLC, fully satisfying the stringent injection specifications for STCF's electron beams.

In contrast to other on-axis electron and positron injector facilities, STCF's requirements are more stringent in aspects such as energy stability and emittance control. For example, the beam energy stability requirements for STCF are critical to ensure accurate collision events for tau-charm physics research. In terms of emittance, the ultralow values demanded by STCF are essential for achieving the desired high luminosity. These unique and more demanding requirements drive the innovation in our injector design, setting it apart from existing facilities and positioning it as a novel solution in the field of particle collider injection systems.

The subsequent sections will elaborate on a physical design for such a high-charge injector, meticulously crafted to meet the demands of STCF's on-axis swap-out injection scheme. The beamline layout and design parameters of the proposed scheme are introduced initially. Subsequently, the preliminary design and analysis of longitudinal bunching and transverse focusing within

the bunching system are first carried out through analytical calculations using an in-house one-dimensional (1D) beam dynamics simulation code developed in MATLAB. Then, the bunching system's physical design is implemented via dedicated beam dynamics software, with full consideration of space-charge forces, wakefields, and alignment errors. Finally, start-to-end simulations of the entire linac system are conducted based on this physical design—incorporating the same realistic effects—to verify the integrated scheme's feasibility under practical operational conditions.

II. OVERVIEW OF THE STCF INJECTOR LINAC FOR THE SWAP-OUT INJECTION OF ELECTRON BEAM

Figure 1 illustrates the entire STCF system sketch under the on-axis swap-out injection scheme, in which the injector includes the separate acceleration of electron and positron beams. In this setup, positrons are generated by directing an 11.6 nC, 90 Hz electron beam onto a target after it is accelerated to 2.5 GeV. The positrons are collected by a capture system, accelerated to 1 GeV, and accumulated in an accumulation ring to form bunches with a charge of 8.5 nC. One fully damped bunch is extracted per pulse and accelerated in the main linac, alternately with the electron beam, to a maximum energy of 3.5 GeV before injection into the positron ring of the collider. In contrast, the electron beam is accelerated to 1.0–3.5 GeV and injected directly into the electron ring of the collider, which is the primary focus of this study.

TABLE II. The main electron parameters of the STCF injector under swap-out scheme [21].

Parameters	Value	Unit
Energy	3.5	GeV
Charge	~8.5	nC
Accelerator frequency	2998.2	MHz
Injection frequency	30	Hz
Energy spread	≤ 0.5	%
Normalized emittance	≤ 210	mm mrad

To achieve the high-brightness requirements of the STCF swap-out injection scheme, the linear accelerator system, comprising the bunching and accelerating sections, must generate high-charge electron bunches characterized by low energy spread and low emittance. The design specifications for the electron beam injector are summarized in Table II, while the beamline layout is illustrated in Fig. 2. It should be noted that the electron-beam injector is designed to provide a single bunch with a charge of up to 8.5 nC, allowing for direct on-axis injection into the collider ring. The generation of such a high-charge single bunch is challenging for an S-band photocathode injector. Considering both the overall system cost and

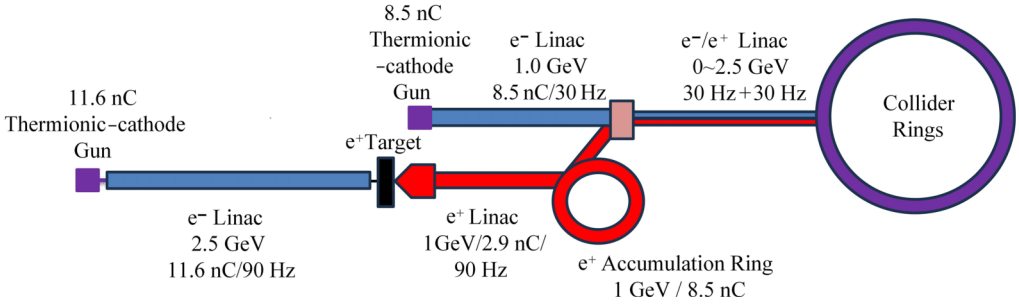


FIG. 1. The STCF layout under the swap-out injection scheme.

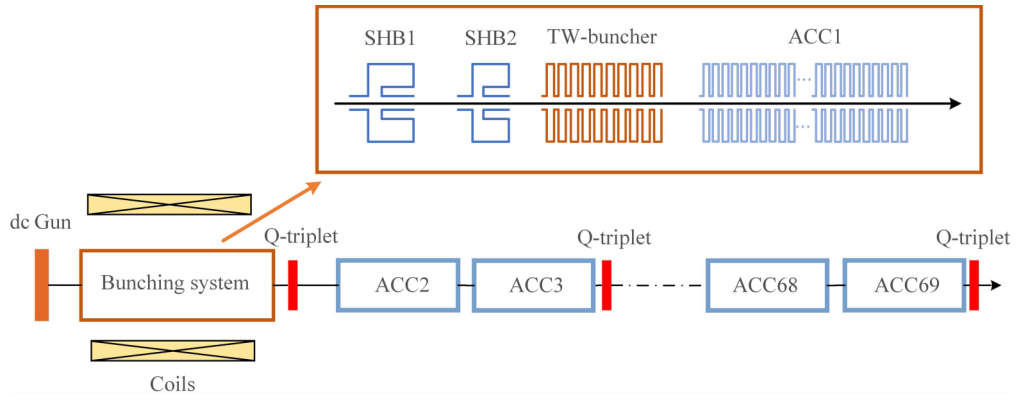


FIG. 2. The beamline layout of the STCF electron injector under the swap-out injection.

operational stability, a thermionic electron gun has been chosen in this study to emit the initial high-current electron beam. During the subsequent longitudinal bunching process with a high compression ratio, nonlinear changes in the longitudinal phase space of the low-energy high-current electron beam, along with the effects of strong space charge, impose significant design challenges on the injector. Furthermore, to ensure the final output bunch properties of the injector, the design of the injector, particularly the bunching system, must carefully consider the strong coupling between transverse and longitudinal performances. This constitutes one of the main contributions of the present study.

As shown in Fig. 2, a long-pulse electron beam generated by a thermionic electron gun is first captured and compressed by the bunching system. It is then accelerated to a maximum energy of 3.5 GeV by a series of 68 standard SLAC-like linacs [22]. Between each pair of linacs, a triplet of quadrupole magnets (Q-triplet) is installed to constrain the transverse dimensions and emittance of the beam. Additionally, these quadrupole magnets can be integrated with downstream insertable detectors to perform emittance measurements based on the quadrupole scanning method [23].

The bunching system consists of a thermionic electron gun, two subharmonic cavity bunchers (SHBs) [24], a traveling-wave buncher (TW-buncher), and a SLAC-like linac (ACC1) with a length of 3 m. The operating frequencies of the SHBs are set at $1/18$ and $1/6$ of the fundamental frequency used by the TW-buncher and main accelerators. The beamline is enclosed by solenoid coils to enhance transverse beam confinement. The SHBs compress the initial beam from the gun to approximately $1/4$ of the wavelength of the subsequent TW linacs, ensuring that the bunch is fully accepted by the TW-buncher. This TW-buncher employs a variable-phase, variable-gradient disk-loaded waveguide structure, further compressing the bunch length to about 10 ps (rms) and increasing its energy to over 10 MeV. The bunch then enters ACC1, where it is accelerated to around 62 MeV. To mitigate the effects of strong space charge and the resulting transverse and longitudinal coupling under intense bunching conditions, solenoid coils are also installed around ACC1.

The TW-buncher and all subsequent constant-gradient TW linacs operate in the $2\pi/3$ mode at a frequency of 2998.2 MHz. The TW-buncher has a total length of 1.2 m, with a nonuniform structure characterized by variable phase and variable gradient. Optimization of the phase velocity and field gradient for each cell enhances bunching performance, thereby improving capture ratio and system transmission efficiency. Each subsequent linac comprises 90 optic-velocity cells with an average accelerating gradient of 17 MV/m, resulting in an energy gain of approximately 51 MeV. In practice, the initial linac, in conjunction with its upstream TW-buncher, delivers a beam energy exceeding 60 MeV. The influence of subsequent linacs on bunch length modulation is minimal, allowing optimal positioning of the bunch around the maximum acceleration phase for enhanced longitudinal performance. Additionally, steering coils or correction magnets will be designed and installed downstream of the solenoid coils or at the exit of each linac to correct beam trajectories.

III. PRELIMINARY DESIGN OF BUNCHING SYSTEM UNDER SINGLE-PARTICLE MODEL

As previously noted, the electron injector for STCF swap-out injection requires high-quality electron bunches. The nanosecond-scale pulses generated by the thermionic gun must be compressed to the picosecond range via the bunching system—an essential step for achieving high-charge bunches while maintaining acceptable energy spread and transverse emittance. Common in high-charge injectors, such bunching schemes typically integrate components including SHBs and TW-bunchers [25].

This section introduces the fundamental principles of the STCF bunching system (comprising SHB1, SHB2, a TW-buncher, and ACC1) and presents its preliminary design using a single-particle model. The primary objective is to theoretically analyze the system's longitudinal bunching performance, thereby preliminarily determining the beamline layout and key component parameters to inform subsequent beam dynamics-based physical design. Given that the bunching system incorporates various rf components (SHBs and a TW-buncher), both their structural and rf parameters exert a decisive influence on longitudinal bunching efficiency. To address this typical multiobjective optimization challenge, the NSGA-III algorithm using analytical methods is adopted instead of parameter scanning, ensuring optimal parameter configurations while enhancing optimization efficiency.

A. Fundamental theory and preliminary design of SHB

When a long pulse beam enters an SHB, electrons at different longitudinal positions acquire varying energies due to the harmonic effects of the rf fields, resulting in velocity modulations along the beam. During the drift process following the SHB, these velocity differences induce phase modulations. By adjusting the rf phase of the SHB such that the field strength experienced by the head electrons is weaker than that encountered by the tail electrons, longitudinal bunching can be achieved, as the tail electrons catch up with the head. This effect is particularly pronounced when the bunch head is subjected to a decelerating field while the tail experiences an accelerating field, a phenomenon referred to as ballistic bunching or velocity bunching [26]. By optimizing the SHB structure with a drift tube and then adjusting the

SHB's accelerating voltage and phase, the desired prebunching result can be achieved.

The aforementioned theories can be conveniently illustrated using analytical formulas. Consider two electrons, each with an initial velocity v_0, encountering rf phases φ_1 and φ_2 upon entering the SHB. Their energy gains are represented as $eV_g \sin\varphi_1$ and $eV_g \sin\varphi_2$, respectively [27]. Consequently, the velocities of the two electrons after traversing the SHB, denoted as v_1 and v_2, can be expressed as follows:

$$\begin{cases} v_1 = c\sqrt{1-\frac{(m_0c^2)^2}{(m_0c^2+eV_a+eV_g\sin\varphi_1)^2}} \\ v_2 = c\sqrt{1-\frac{(m_0c^2)^2}{(m_0c^2+eV_a+eV_g\sin\varphi_2)^2}} \end{cases}, \tag{1}$$

where V_g represents the maximum voltage amplitude of the SHB, while eV_a denotes the initial kinetic energy of the electrons, corresponding to v_0. Note that, the rest energy of the electron is expressed as m_0c^2 with m_0 and c denoting the electron mass and light speed, respectively.

If the two electrons drift downstream of the SHB by a distance of L_0, the phase difference between them will evolve from $\Delta\varphi(0) = |\varphi_2 - \varphi_1|$ to,

$$\Delta\varphi(L_0) = \left|\varphi_2 - \varphi_1 + \omega L_0\left(\frac{1}{v_2} - \frac{1}{v_1}\right)\right|, \tag{2}$$

where ω is the rf angular frequency. It is clear that when $\varphi_1 \neq \varphi_2$, $v_1 \neq v_2$, indicating that electrons entering the SHB at different phases will exit with different velocities. Then, by adjusting the SHB phase, velocity bunching can be observed. Note that, the actual bunching effect depends on the drift length L_0 as well.

As outlined in Sec. II and detailed in Table II, the proposed bunching system comprises two SHBs and one TW-buncher, utilizing current technologies in thermionic-cathode guns [28,29] to achieve an adequate compression ratio.

For the preliminary beamline design incorporating these bunching elements, the third-generation multiobjective genetic algorithm, NSGA-III [30,31], is employed in conjunction with a single-particle model. The primary design objective is to utilize the two SHBs to achieve a high bunching ratio while minimizing energy spread. Key optimization parameters include the acceleration voltages and rf phases of the SHBs, as well as the drift distances between them. Constraints are determined by the operating frequencies of the SHBs and the input bunch length of 1.3 ns—which corresponds to the output distribution from the High Energy Photon Source (HEPS) electron gun, and is assumed to be a uniform distribution in our in-house 1D simulation code [32].

For instance, by selecting appropriate structural and rf parameters, a solution can be attained with a bunch length of 26.72° (in terms of phase width refers to the fundamental frequency of the TW accelerating structures, which is 2998.2 MHz as listed in Table III). and an energy spread of 7.43%, as illustrated in Fig. 3(a). The corresponding longitudinal phase spaces (LPSs) at various positions along the beamline are shown in Fig. 3(b). The optimization process using the NSGA-III algorithm ensures that all particles are bunched into the same rf period, resulting in a 100% particle capture rate.

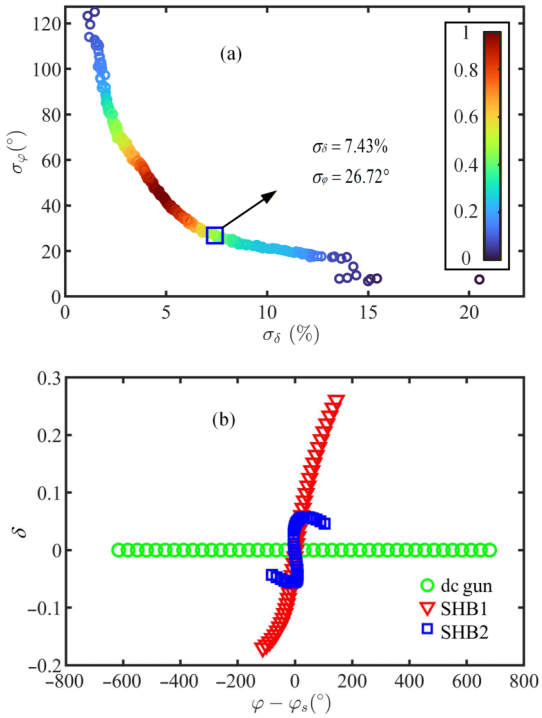


FIG. 3. (a) Pareto front generated by NSGA-III. (b) Longitudinal phase spaces at the exit of the dc gun, SHB1, and SHB2.

B. Preliminary design of TW-buncher

According to the above simulation results, the bunch length reaches 26.72° after prebunching with SHB1 and SHB2. At this stage, the beam energy is only a few hundred keV, while the peak current exceeds 300 A, leading to significant space charge effects. Consequently, an additional TW-buncher is required to rapidly increase the beam energy and further reduce the bunch length. In designing the TW accelerating structure utilizing

TABLE III. The design parameters of the injector system.

	Frequency (MHz)	Energy gain (MeV)	Length (m)
SHB1	166.57	0.12	0.80
SHB2	499.70	0.25	0.30
TW-buncher	2998.20	11	1.20
ACC	2998.20	51	3

an iris-loaded waveguide, it is essential to establish the relationship between the electric field strength E and the rf power P as a function of the longitudinal position z. Considering the beam loading effect, the relevant theoretical equations can be expressed as follows [33]:

$$\begin{cases} E(z) = \sqrt{2\alpha Z_s P(z)} \\ \frac{\mathrm{d}P(z)}{\mathrm{d}z} = -2\alpha P(z) - IE(z) \end{cases}, \tag{3}$$

where α and Z_s represent the attenuation factor and shunt impedance, respectively, and I denotes the average beam current. The distribution of $E(z)$ must be designed to meet the quality requirements for the output beam, and corresponding longitudinal motions of the electrons can be solved by [33]:

$$\begin{cases} \frac{\mathrm{d}\gamma}{\mathrm{d}z} = -\frac{eE(z)}{m_0c^2}\sin\varphi \\ \frac{\mathrm{d}\varphi}{\mathrm{d}z} = \frac{2\pi}{\lambda}\left(\frac{1}{\beta_p} - \frac{\gamma}{\sqrt{\gamma^2-1}}\right) \end{cases}, \tag{4}$$

where γ is the relative energy of the electron. φ, λ, and β_p represent the rf phase, rf wavelength, and phase velocity of the TW-buncher cell, respectively.

The phase oscillations within the TW-buncher obtained from the single-particle simulations are illustrated in Fig. 4(a). Notably, variable phase velocities and accelerating gradients are employed to the first 9 cells, enabling further compression of the bunch as it traverses the TW-buncher. The remaining 27 cells are configured as light-speed structures, divided into two groups based on different acceleration gradients, enabling rapid energy boost to mitigate space charge effects. For comparative analysis, the LPSs before and after the TW-buncher are presented in Fig. 4(b).

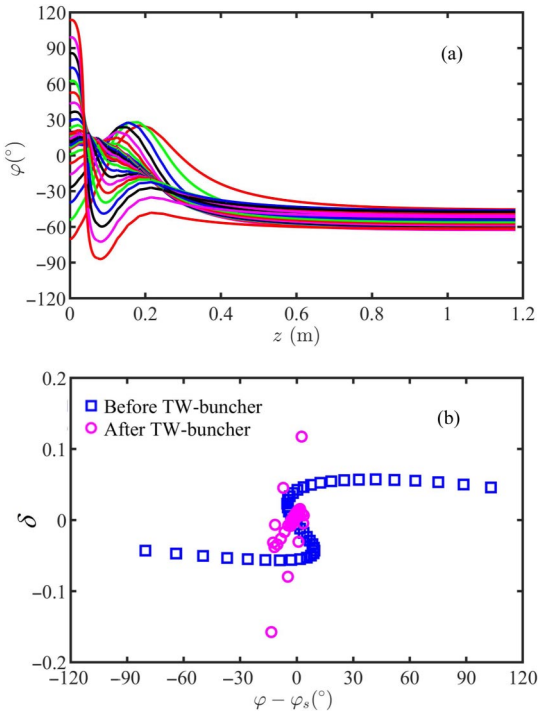


FIG. 4. (a) Phase oscillations along the longitudinal position in the TW-buncher. (b) LPSs before and after the TW-Buncher.

It is important to note that the swap-out injection of the STCF is characterized by high current and large charge, resulting in significant space charge effects within the bunching system. Particularly at the entrance of the TW-buncher, the phase width of the 8.5 nC bunch occupied is expected to compress to approximately 6°, referring to 2998.2 MHz. Thus, strong phase oscillations are inevitable, as illustrated in Fig. 4(b). Since the beam energy is below 1 MeV at this stage, strong focusing magnetic fields must be applied to mitigate transverse expansion induced by the pronounced space charge effects.

IV. TRANSVERSE OPTIMIZATION AND BEAM DYNAMICS SIMULATIONS

The single-particle simulations discussed earlier focus only on the longitudinal bunching characteristics. Therefore, it is crucial to conduct beam dynamics simulations that comprehensively assess the evolution of both transverse and longitudinal performances, while adequately accounting for the effects of space charge in the actual design.

A. Transverse optimization using solenoid coils

As previously noted, to maintain the transverse performance of the beam, it is necessary to install focusing coils surrounding the bunching system. The equation governing the transverse motions of electrons in the rf section can be expressed as follows:

$$\frac{\mathrm{d}}{\mathrm{d}z}(\beta\gamma R') + \frac{e}{m_0c^2}Q(z)R = \frac{\varepsilon_r^2}{\beta\gamma R^3}, \tag{5}$$

where β represents the electron relative velocity, R and R' denote the beam radius and its first derivative, respectively, Q signifies the radial focusing force coefficient, and ε_r indicates the normalized radial emittance, defined as $\beta\gamma$ times the geometric emittance. For a group of electrons with identical longitudinal conditions, by assuming ε_r that characterizes their collective transverse properties remains constant, Eq. (5) can also be rewritten as follows:

$$\frac{\mathrm{d}^2R}{\mathrm{d}z^2} = -\frac{1}{\beta^2\gamma}\frac{\mathrm{d}\gamma}{\mathrm{d}z}\frac{\mathrm{d}R}{\mathrm{d}z} - \frac{eR}{\beta\gamma m_0c^2}Q(z) + \frac{\varepsilon_r^2}{\beta^2\gamma^2R^3}. \tag{6}$$

During the drift process, the first term on the right side of the equation is zero owing to the invariance of γ, enabling a straightforward solution for the transverse envelope of the beam. In contrast, within the rf section,

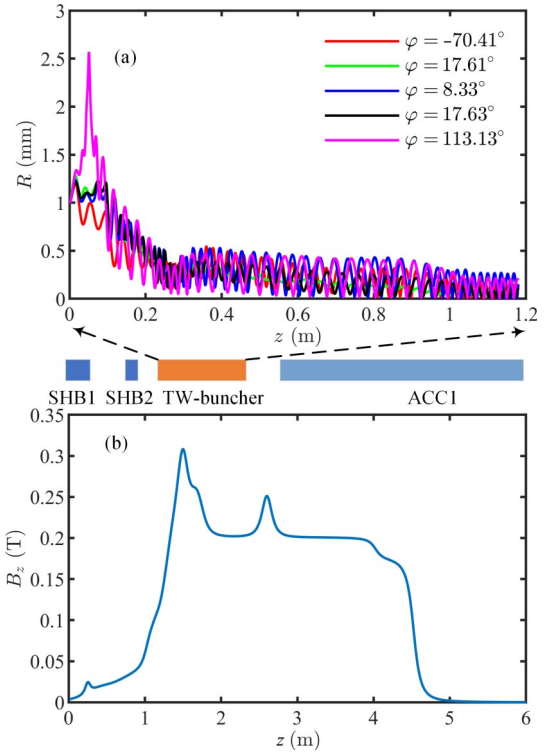


FIG. 5. (a) Beam transverse motions in the TW-buncher. (b) Axial magnetic field distribution in the bunching system.

both β and γ vary with z, necessitating the incorporation of the longitudinal motion equations to determine the beam envelope. Taking the TW-buncher as an example, the beam envelope can be derived by combining Eqs. (4) and (6). The solutions are illustrated in Fig. 5(a), where different colors and line styles represent particles with varying initial phases. The corresponding axial magnetic field distribution used in the calculations is displayed in Fig. 5(b).

Throughout the bunching system, the maximum magnetic field reaches 0.3 T, located at the front of the TW-buncher. The initial phases and energies assigned to the electrons in the calculations are sourced from the outputs of SHB2, as shown in Fig. 3(b). For clarity, Fig. 5(a) presents only five particles that span the range of phases, each with an initial transverse deviation of 1 mm. It can be observed that the transverse deviations of the electrons entering the TW-buncher under different initial conditions are constrained within 0.75 mm.

B. Beam dynamics simulations for bunching system

The single-particle simulations effectively simplify the adjustment and optimization of the injector beamline, thereby facilitating the rapid development of the preliminary layout design. Therein, the longitudinal bunching and transverse focusing characteristics are analyzed independently. However, for designing a high-current, large-charge bunching system, it is imperative to conduct comprehensive beam dynamics simulations, considering space charge effects and the interactions between transverse and longitudinal behaviors. In this section, the physical design of the STCF injector will be performed using the multiparticle simulation software Parmela [34], which employs space charge forces in cylindrical meshes. The initial beam parameter distribution is from the HEPS thermionic gun, which includes 300,000 particles with a full-width at half-maximum (FWHM) pulse length of 1.3 ns and a total charge of 8.5 nC. The longitudinal and transverse phase spaces are shown in Figs. 10(a) and 10(d).

For the bunching system, beam dynamics simulations are conducted based on the system setup from the above preliminary design. The evolutions of longitudinal and transverse performances are illustrated in Figs. 7(a) and 7(b). Key parameters for the rf sections are summarized in Table III.

Significant variations of the beam performances occur primarily in the preceding segment of the TW-buncher and the sections before it, while the changes after it are relatively gradual. This observation is consistent with the analysis presented in Sec. III. Furthermore, after entering SHB1, the energy spread increases significantly and exhibits fluctuations, but once the bunching process is completed at the front of the TW-buncher, the energy spread begins to decrease steadily. Note that, to achieve better compression in the TW-buncher, the beam is in the decelerating phase within the first few cells, where phase velocity matching is sacrificed to realize high capture efficiency. Figure 6(c) illustrates such variations in energy and LPSs within the TW-buncher. At several marked positions in the figure, the energy first increases and then decreases, which corresponds to the initial reduction followed by an increase in bunch length shown in Fig. 6(a).

In the case of transverse performances, both horizontal and vertical sizes remain relatively stable at around 1.5 mm due to the confinement provided by the focusing coils; the normalized transverse emittance shows only a slight increase, reaching just above 60 mm mrad. This indicates that the transverse expansion caused by significant space charge forces can be mitigated, reducing the strong coupling between longitudinal and transverse performances. Simulation results at the exit of the bunching system are detailed in Table IV. Since the quality of the bunch head containing the vast majority of particles plays a decisive role in injection efficiency, an energy spectrum truncation is implemented at $\pm 3\sigma_\delta$ in subsequent calculations. This approach retains about 95% of electrons, while the residual low-energy tail particles can be efficiently removed using collimators in the downstream transport line of the main linacs. So that, the design and simulation results listed in the Tables IV and V, such as the normalized (Nor.) emittance, energy spread, bunch length, and transverse sizes represent the root mean square (rms) values of the bunch head containing 95% of electrons.

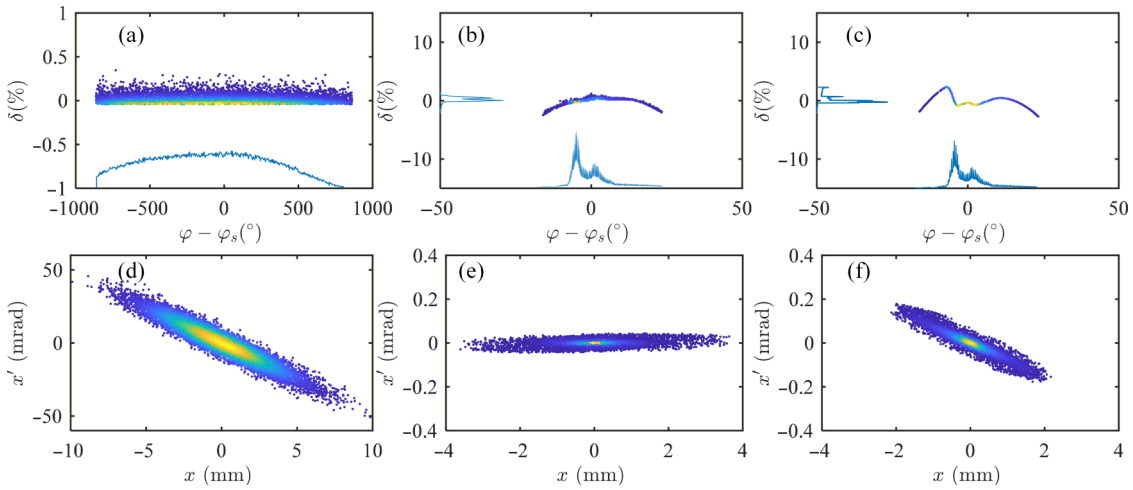


FIG. 6. Longitudinal phase space at exit of (a) electron gun, (b) injector (without errors), (c) injector (with errors); transverse phase space at exit of (d) electron gun, (e) injector (without errors), (f) injector (with errors).

C. Beam dynamics simulations for main accelerators

As discussed in the previous section, through the optimization of the bunching system design, the bunch length is compressed to approximately 6 ps (rms), at which point the electron relative velocity β reaches 0.999. Consequently, the bunch length remains nearly constant in the subsequent acceleration sections. Since the primary function of the light-speed linacs is to rapidly boost the energy up to 3.5 GeV for the collider rings, the bunch is typically positioned at the maximum acceleration phase in most linac sections, which may lead to an increase in energy spread. To mitigate this deterioration, it is crucial to adjust the rf phases of several linacs to minimize energy spread, albeit at a slight cost to the energy gain of those linacs. This loss can be compensated by increasing the feed-in power of the terminal linacs.

Moreover, to meet the specifications for the STCF swap-out injection, further constraints on beam transverse emittance and dimensions are necessary. At high-energy stages, the adjustment capabilities of the solenoid coils regarding transverse performances are significantly limited. Therefore, a Q-triplet is positioned between each pair of linacs, which serves a dual purpose: constraining the transverse dimensions to below 1 mm and facilitating the matching of both horizontal and vertical beam sizes.

To validate the designed performance of the injector, comprehensive beam dynamics simulations for the light-speed linacs are conducted using Parmela. The calculated evolutions of the main beam parameters are illustrated in Fig. 8. As shown in Fig. 8(a), optimizing the rf phases allows the bunch length to be maintained at approximately 6.13 ps throughout the entire light-speed linac sections, with the energy spread remaining around 0.41% by the end of the process. Furthermore, the transverse performance variation curves presented in Fig. 8(b) indicate that both horizontal and vertical dimensions do not exceed 0.8 mm at the exit. Although a slight difference in normalized emittance between the two directions is noted, both remain below 66 mm mrad.

TABLE IV. The beam parameters at the bunching system and main linac outlet.

	Beam dynamics results	
Parameters	Bunching system	Main linac
Charge, Q	8.5 nC	8.5 nC
Energy, E_s	61.97 MeV	3.51 GeV
Normalized emittance, $\epsilon_{x,y}$	61.18 mm mrad	65.63 mm mrad
rms energy spread, σ_δ	0.9%	0.41%
rms bunch length, σ_t	6.13 ps	6.13 ps
rms transverse sizes, $\sigma_{x,y}$	1.53 mm	0.78 mm

TABLE V. Main beam parameters of STCF injector.

Parameters	Design targets	Simulation results (after error corrections)
Charge, Q	8.5 nC	8.5 nC
Energy, E_s	3.5 GeV	3.51 GeV
Normalized emittance, $\epsilon_{x,y}$	≤210 mm mrad	68.39 mm mrad
rms energy spread, σ_δ	≤0.5%	0.46%
rms bunch length, σ_t	≤10 ps	6.13 ps
rms transverse size, $\sigma_{x,y}$	≤1 mm	0.78 mm

V. MISALIGNMENT-INDUCED WAKEFIELDS IN THE MAIN LINACS

In general, when a high-current, short bunch passes through varying structures such as a traveling-wave accelerator, both long-range and short-range wakefields

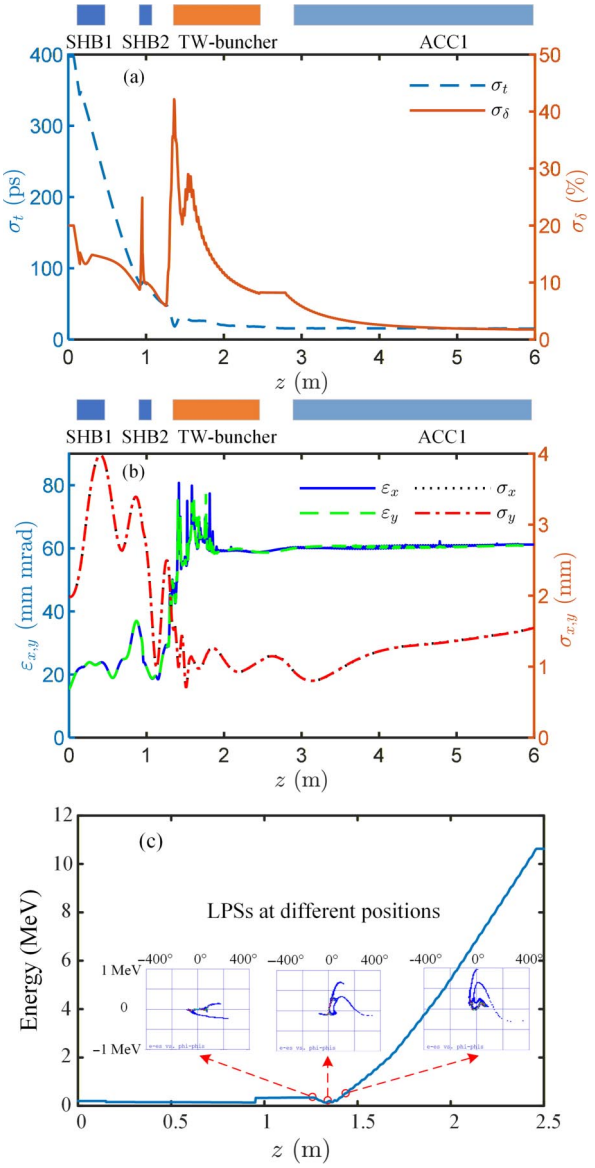


FIG. 7. Longitudinal (a) and transverse (b) performance variations in the bunching system, and kinetic energy change in the SHBs and TW-buncher (c).

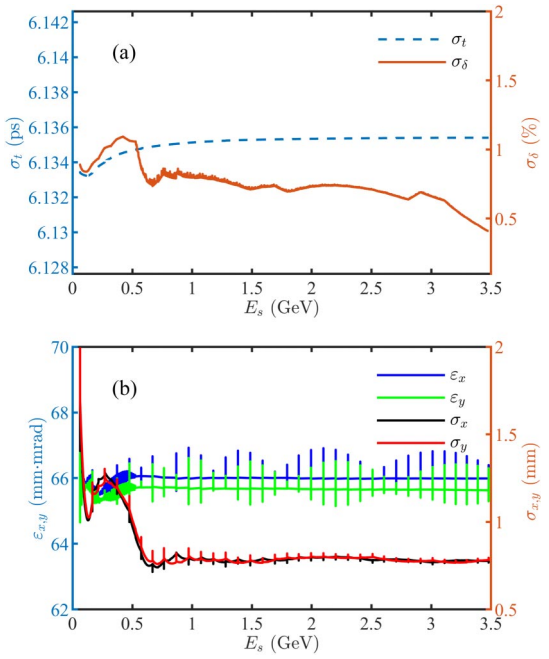


FIG. 8. Longitudinal and transverse parameters at the injector outlet: (a) beam length and energy spread, (b) beam size and normalized emittance.

are excited within the structure. The short-range wakefield, or self-field, acts back on the bunch itself, degrading its internal uniformity. In practice, beamline components—including accelerating structures and magnets—inevitably experience small alignment errors during fabrication and installation. If the beam centroid deviates from the electric or magnetic field center, the resulting transverse wakefields further displace the beam, thereby amplifying downstream wakefield effects and causing significant deterioration in both transverse and longitudinal beam quality. Therefore, it is essential to analyze the combined impact of wakefields and alignment errors and to implement the BBA [35] in order to mitigate beam performance degradation.

Since the bunch parameters fluctuate most significantly in the bunching system, where the effect of wakefields is relatively small, this study primarily focuses on the main accelerating section downstream. In typical beamlines, mechanical alignment techniques—such as optical-telescope methods or laser trackers—are employed to constrain component center errors to within 0.1 mm and tilt errors to within 1 mrad [36]. Furthermore, by equipping each triplet in the layout, as shown in Fig. 2, with a beam position monitor and a set of steering magnets, a BBA scheme can be implemented.

To simulate the effects of alignment errors and wakefields, random center offsets with an rms value of 0.1 mm and tilt errors with an rms value of 1 mrad are assigned to each beamline element. Additionally, a random jitter of up to $\pm 0.1\%$ is applied to both the accelerating and magnetic fields' amplitude, and an rms 0.2° phase jitter is applied to the bunching system and ACCs. The wakefield distributions in the linacs are computed using ECHO [37]. Since the STCF electron injector operates at 30 Hz and only injects one bunch at a time, the interval between successive bunches far exceeds the wakefield decay time, and thus, only the short-range self-field is considered. ELEGANT [38] simulations are then used to calculate the beam orbits under the combined influence of wakefields and alignment errors, as shown in Fig. 9(a). The beam orbit deviation grows steadily during transport, reaching nearly 10 mm at the injector exit, leading to a doubling or greater of the transverse emittance, as indicated by the red and black curves in Fig. 10(b). Meanwhile the bunch length and

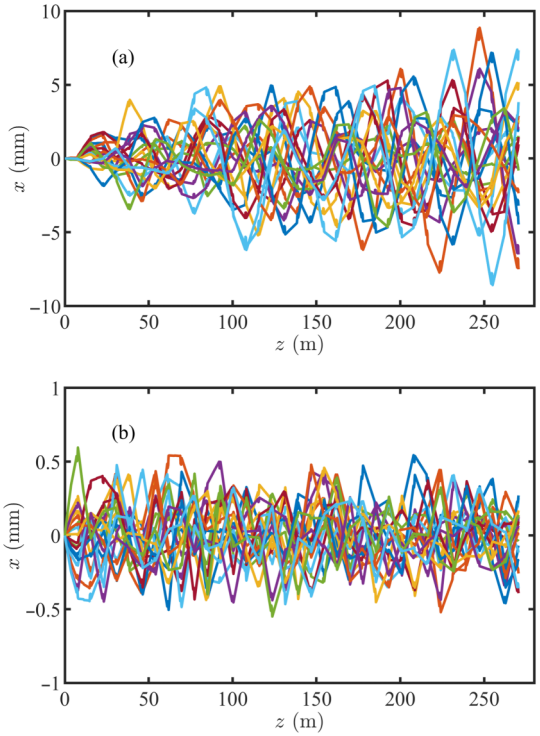


FIG. 9. Beam orbits affected by wakefield effects and alignment errors (a), and those after corrections via the BBA algorithm (b).

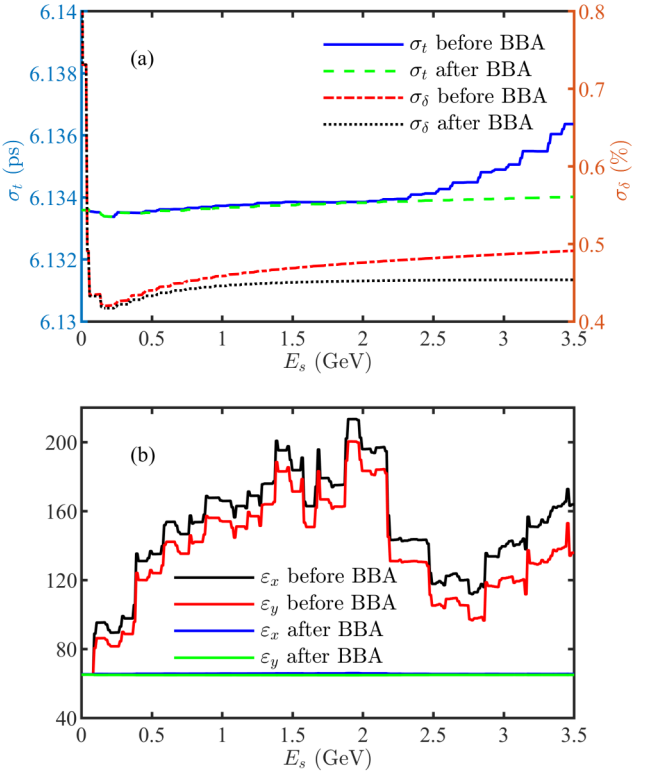


FIG. 10. Beam parameters variations after BBA correcting the wakefield effects and alignment errors: (a) beam length and energy spread, (b) transverse normalized emittance.

energy spread slightly increase to 6.136 ps and 0.49%, respectively, as shown by the blue and red dash-dotted lines in Fig. 10(a).

The application of the BBA algorithm in ELEGANT can reduce the orbit offsets to within 0.1 mm (rms), as seen in Fig. 9(b). The transverse and longitudinal phase spaces of the injector output beam are shown in Figs. 6(c) and 6(f), while the phase spaces without wakefields and alignment errors are also provided in Figs. 6(b) and 6(e) for comparisons. Additionally, it is obvious from Fig. 10 that although the corrected longitudinal and transverse phase spaces exhibit significant deviations compared to the error-free case, both the transverse and longitudinal beam parameters are similarly well-controlled via BBA algorithm with error considered.

To fulfill the swap-out injection requirements at the STCF collider rings, comprehensive theoretical analysis and beam dynamics simulations are performed to deliver the physical design for the electron injector. Space-charge forces, wakefield interactions, and misalignment-induced perturbations are fully considered.

The NSGA-III algorithm integrated with single-particle models efficiently optimizes the bunching system, whose multiple rf components possess interdependent parameters. In the main accelerating section, the BBA algorithm corrects orbit deviations induced by wakefield effects and alignment errors. Start-to-end simulations incorporating realistic error budgets demonstrate that the proposed design meets the STCF swap-out injection requirements, with final beam parameters summarized in Table V.

In summary, this work demonstrates that a systematic, comprehensive optimization methodology—integrating NSGA-III multiobjective algorithms, full consideration of space-charge and wakefield effects—enables a thermionic-gun injector without a beam scraper to deliver high-charge bunches with excellent beam quality. The design overcomes traditional thermionic-cathode limitations while leveraging their proven stability, robustness, and cost-effectiveness. The methodology provides transferable insights for similar high-charge linac injectors. Note that, although the transmission efficiency of 100% is a result obtained from beam dynamics simulations, high-precision detailed simulations can also, to a large extent, directly reflect the performance indicators that the system design can achieve.

The present study is limited to the beam physics design stage, vacuum chamber engineering, diagnostic integration, rf structure tolerances, and comprehensive beam halo analysis are deferred to the subsequent engineering design phase. However, the proposed design and optimization methodology for high-charge injectors not only addresses STCF-specific requirements but also provides transferable insights for similar linear accelerator configurations in advanced light sources or collider applications.

ACKNOWLEDGMENTS

This work is supported by the National Key R&D Program of China under Contract No. 2022YFA1602202, the National Natural Science Foundation of China (No. 12341501 and No. 12575164), the international partnership program of the Chinese Academy of Sciences Grant No. 211134KYSB20200057 and the STCF key technology research and development project. We thank the University of Science and Technology of China and Hefei Comprehensive National Science Center for their strong support on the promotion and development of the STCF project. We thank Dr. Cai Meng at the Institute of High Energy Physics of the Chinese Academy of Sciences for providing electron-gun outputs, Dr. Yao Lu and Dr. Jian Pang at University of Science and Technology of China for their stimulating discussions.

DATA AVAILABILITY

There are no publicly available research data or software supporting this manuscript. Requests for further information or data should be sent to the authors.

[1] M. Ablikim *et al.*, BESIII Collaboration, Observation of a state $X(2600)$ in the $\pi^+\pi^-\eta'$ system in the process J $J/\psi \to \gamma\pi^+\pi^-\eta'$, Phys. Rev. Lett. **129**, 042001 (2022).

[2] M. Ablikim *et al.*, Observation of charged κ in $J/\psi \to K^*(892)^\mp K_S\pi^\pm$, $K^*(892)^\mp \to K_S\pi^\mp$ at BESII, Phys. Lett. B **698**, 183 (2011).

[3] M. Ablikim *et al.*, BESIII, Observation of $\alpha_0^0(980) - f_0(980)$ mixing, Phys. Rev. Lett. **121**, 022001 (2018).

[4] T. Xiang, X.-D. Shi, D.-Y. Wang, and X.-R. Zhou, Sensitivity study of the charged lepton flavor violating process $\tau \to \gamma\mu$ at STCF, Eur. Phys. J. C **83**, 908 (2023).

[5] J. Z. Bai *et al.*, Measurement of the mass of the tau lepton, Phys. Rev. Lett. **69**, 3021 (1992).

[6] G. S. Abrams *et al.*, The mark-II detector for the SLC, Nucl. Instrum. Methods Phys. Res., Sect. A **281**, 55 (1989).

[7] D. Bernstein *et al.*, The mark-III spectrometer, Nucl. Instrum. Methods Phys. Res., Sect. A **226**, 301 (1984).

[8] Y. U. Jeong, K.-H. Jang, S. Bae, V. Pathania, J. Mun, and K. Lee, Prospects of a terahertz free-electron laser for field application, J. Korean Phys. Soc. **80**, 367 (2022).

[9] M. Achasov *et al.*, STCF conceptual design report (Volume 1): Physics & detector, Front. Phys. **19**, 14701 (2024).

[10] J. Tang, Accelerator design and R&D efforts for Super Tau-Charm Facility, in *Proceedings of the 42nd International Conference on High Energy Physics, PoS(ICHEP2024)810*, Prague, Czech Republic (2024), https://indico.cern.ch/event/1291157/contributions/5889969/.

[11] J. M. Gibson, R. B. Fenner, G. Long, M. Borland, and G. Decker, *APS Science 2006* (Report No. ANL-06/23). Argonne National Laboratory, Advanced Photon Source (2007), 10.2172/962874.

[12] Y. Jiao, G. Xu, X.-H. Cui, Z. Duan, Y.-Y. Guo, P. He, D.-H. Ji, J.-Y. Li, X.-Y. Li, C. Meng, Y.-M. Peng, S.-K. Tian, J.-Q. Wang, N. Wang, Y.-Y. Wei, H.-S. Xu, F. Yan, C.-H. Yu, Y.-L. Zhao, and Q. Qin, The HEPS project, J. Synchrotron Radiat. **25**, 1611 (2018).

[13] H. Takaki, N. Nakamura, Y. Kobayashi, K. Harada, T. Miyajima, A. Ueda, S. Nagahashi, M. Shimada, T. Obina, and T. Honda, Beam injection with a pulsed sextupole magnet in an electron storage ring, Phys. Rev. ST Accel. Beams **13**, 020705 (2010).

[14] A. Abada *et al.*, FCC-Ee: The Lepton Collider, Eur. Phys. J. ST **228**, 261 (2019).

[15] C. Gough and M. Mailand, Septum and kicker systems for the SLS, in *Proceedings of the Particle Accelerator Conference, Chicago, IL, 2001* (IEEE, New York, 2001), p. 3741.

[16] M. Aiba, M. Böge, F. Marcellini, Á Saá Hernández, and A. Streun, Longitudinal injection scheme using short pulse kicker for small aperture electron storage rings, Phys. Rev. Accel. Beams **18**, 020701 (2015).

[17] SLAC Linear Collider Design Group, SLAC Linear Collider Conceptual Design Report, Stanford Linear Accelerator Center, Menlo Park (1980), https://digital.library.unt.edu/ark:/67531/metadc1056595/.

[18] J. T. Seeman, The Stanford Linear Collider, in *Proceedings of the Linear Accelerator Conference* (JaCoW, Albuquerque,
New Mexico, USA, 1990), https://proceedings.jacow.org/l90/papers/mo101.pdf.

[19] SuperKEKB Design Group, SuperKEKB design report, High Energy Accelerator Research Organization (KEK), Tsukuba, Japan (2020), https://www-linac.kek.jp/linac-com/report/skb-tdr/.

[20] J. Gao, CEPC technical design report: Accelerator, Radiat. Detect. Technol. Methods **8**, 1 (2024).

[21] A. Zhang, D. Gu, T. Hu, G. Pei, J. Tang, and Y. Yuan, STCF injector and positron source design, in *Proceedings of the 70th ICFA Advanced Beam Dynamics Workshop on High Luminosity Circular e^+e^- Colliders*, JACoW(eeFACT2025 TUB04), Tsukuba, Ibaraki, Japan (2025), https://indico.jacow.org/event/75/contributions/6733/.

[22] T.-N. Hu, H.-M. Wang, Y.-F. Zeng, H.-J. Xu, L. Chen, G.-Y. Feng, and Y.-J. Pei, Fault locating for traveling-wave accelerators based on transmission line theory, Nucl. Sci. Tech. **34**, 116 (2023).

[23] Y.-F. Zeng, H. Hu, and T.-N. Hu, Improvement and correction for transverse emittance diagnosis based on Q-scanning techniques, Nucl. Sci. Tech. **36**, 38 (2025).

[24] S. Hajari, S. H. Shaker, and S. Doebert, Sub-harmonic bunching system of CLIC drive beam injector, ICFA Beam Dyn. Newslett. **62**, 28 (2013).

[25] W. Liu and E. Wang, Optimization of an electron injector for operating high-intensity polarized electron beam, Int. J. Mod. Phys. A **37**, 2250068 (2022).

[26] T. Hu, J. Li, K. Peng, H. Xu, and J. Yang, Study of longitudinal phase space for typical beam injector via analytical method, Nucl. Instrum. Methods Phys. Res., Sect. A **1045**, 167628 (2023).

[27] H. Wiedemann, *Particle Accelerator Physics*, 4th edn. (Springer, New York, 2015), pp. 634–636.
[28] T. Asaka, T. Inagaki, T. Magome, N. Nishimori, Y. Otake, T. Taniuchi, K. Yanagida, and H. Tanaka, Low-emittance radio-frequency electron gun using a gridded thermionic cathode, Phys. Rev. Accel. Beams **23**, 063401 (2020).
[29] X.-Y. Peng, H. Hu, T.-N. Hu, J. Pang, J.-J. Deng, and G.-Y. Feng, Emittance optimization of gridded thermionic-cathode electron gun for high-quality beam injectors, Nucl. Sci. Tech. **37**, 19 (2026).
[30] H.-X. Yin, J.-B. Guan, S.-Q. Tian, and J.-K. Wang, Design and optimization of diffraction-limited storage ring lattices based on many-objective evolutionary algorithms, Nucl. Sci. Tech. **34**, 147 (2023).
[31] Z.-Y. Dai, Y.-C. Nie, Z. Hui, L.-X. Liu, Z.-S. Liu, J.-H. Zhong, J.-B. Guan, J.-K. Wang, Y. Chen, Y. Zou, H.-H. Li, and J.-H. He, Design of S-band photoinjector with high bunch charge and low emittance based on multi-objective genetic algorithm, Nucl. Sci. Tech. **34**, 41 (2023).
[32] S.-C. Wang, D.-Y. He, C. Meng, J.-Y. Li, Z.-S. Zhou, and J.-D. Liu, Development and simulation of a gridded thermionic cathode electron gun for a high-energy photon source, Nucl. Sci. Tech. **34**, 39 (2023).
[33] H.-M. Wang, Y.-F. Zeng, H. Hu, J.-Y. Li, and T.-N. Hu, Design and optimization of a compact high-energy electron source applied to on-site non-destructive testing for electrical equipment, Nucl. Sci. Tech. **37**, 63 (2026).
[34] L. M. Young, "PARMELA," Los Alamos National Laboratory report, LA-UR-96-1835, Los Alamos National Laboratory (2003).
[35] Z. Martí, G. Benedetti, U. Iriso, and A. Franchi, Beam-based alignment using ac excitations, Phys. Rev. Accel. Beams **23**, 012802 (2020).
[36] Z. Man-Zhou, L. Hao-Hu, J. Bo-Cheng, L. Gui-Min, and L. De-Ming, Beam-based alignment of the SSRF storage ring, Chinese Phys. C **33**, 301.
[37] I. Zagorodnov, https://echo4d.de/.
[38] M. Borland, Elegant: A flexible SDDS-compliant code for accelerator simulation., Advanced photon source LS-287 (2000).